Sensitivity enhancement in grating coupled surface plasmon resonance by azimuthal control

F. Romanato[1, 2, 3, 4*], K. H. Lee[2], H. K. Kang[2], G. Ruffato[1,4] and C. C. Wong[2]

[1] Dep. of Physics "G. Galilei", Padua Univ., via Marzolo 8, 35131, Padua, Italy
[2] School of Materials Science and Engineering, Nanyang Technological University, 50 Nanyang Ave, Singapore.
[3] LANN Labboratory for Nanofabrication of Nanodevices, of VenetoNanotech, via San Crispino 106, 35129 Padova, Italy.
[4] TASC National Laboratory, CNR-INFM, 34012 Trieste, Italy
*romanato@tasc.infm.it

Abstract: We present a method for improving the sensing capability of grating coupled surface plasmon resonance (GCSPR) sensors. The grating is rotated azimuthally (φ) until the excitation of double surface plasmon polaritions (SPPs) by a single wavelength is possible. Close to this condition, further tuning of the incident wavelength will merge the double SPPs into a multi-SPP resonance which is angularly broad but spectrally sharp. This is the condition where the momentum vector of the propagating SPP is perpendicular to the incident light momentum. We demonstrate this sensitivity enhancement on a Au grating surface using a dodecanethiol (C12) self-assembled monolayer (SAM). Using this method, a shift in resonance angle as large as 3° can be observed. The simulated sensitivity of this method shows that a sensitivity up to 800°/RIU is achievable, which is one order of magnitude greater than that in a conventional fixed grating ($\varphi = 0°$) as well as the prism-coupled Kretschmann configuration.

©2009 Optical Society of America

OCIS codes: (240.6680) Surface plasmons; (280.4788) Optical sensing and sensors

References and links

1. H. Raether, "Surface Plasmons on Smooth and Rough Surfaces and on Gratings," (Springer-Verlag, 1988).
2. L. S. Jung, C. T. Campbell, T. M. Chinowsky, M. N. Mar, and S. S. Yee, "Quantitative interpretation of the response of surface plasmon resonance sensors to adsorbed films," Langmuir **14**(19), 5636–5648 (1998).
3. I. Lundstrom, "Real-time biospecific interaction analysis," Biosens. Bioelectron. **9**(9-10), 725–736 (1994).
4. W. Lukosz, "Integrated-optical and surface-plasmon sensors for direct affinity sensing. Part II: Anisotropy of adsorbed or bound protein adlayers," Biosens. Bioelectron. **12**(3), 175–184 (1997).
5. K. A. Peterlinz, and R. Georgiadis, "In Situ Kinetics of Self-Assembly by Surface Plasmon Resonance Spectroscopy," Langmuir **12**(20), 4731–4740 (1996).
6. J. Homola, S. S. Yee, and G. Gauglitz, "Surface plasmon resonance sensors: review," Sens. Actuators B Chem. **54**(1-2), 3–15 (1999).
7. A. J. Haes, and R. P. Van Duyne, "A unified view of propagating and localized surface plasmon resonance biosensors," Anal. Bioanal. Chem. **379**(7-8), 920–930 (2004).
8. K. A. Willets, and R. P. Van Duyne, "Localized surface plasmon resonance spectroscopy and sensing," Annu. Rev. Phys. Chem. **58**(1), 267–297 (2007).
9. J. Perez-Juste, I. Pastoriza-Santos, L. M. Liz-Marzan, and P. Mulvaney, "Gold nanorod: systhesis, characterization and application," Coord. Chem. Rev. **249**(17-18), 1870–1901 (2005).
10. C. Yu, and J. Irudayaraj, "Multiplex biosensor using gold nanorods," Anal. Chem. **79**(2), 572–579 (2007).
11. J. Melendez, R. Carr, D. U. Bartholomew, K. Kukanskis, J. Elkind, S. Yee, C. Furlong, and R. Woodbury, "A commercial solution for surface plasmon sensing," Sens. Actuators B Chem. **35**(1-3), 212–216 (1996).
12. B. Liedberg, I. Lundstrom, and E. Stenberg, "Principle of biosensing with an extended coupling matrix and surface plasmon resonance," Sens. Actuators B Chem. **11**(1-3), 63–72 (1993).
13. R. Karlsson, and R. Ståhlberg, "Surface plasmon resonance detection and multispot sensing for direct monitoring of interactions involving low-molecular-weight analytes and for determination of low affinities," Anal. Biochem. **228**(2), 274–280 (1995).
14. J. Homola, I. Koudela, and S. S. Yee, "Surface plasmon resonance sensor based on diffraction gratings and prism couplers: sensitivity comparison," Sens. Actuator B **54**(1-2), 16–24 (1999).

15. D. W. Unfricht, S. L. Colpitts, S. M. Fernandez, and M. A. Lynes, "Grating-coupled surface plasmon resonance: a cell and protein microarray platform," Proteomics **5**(17), 4432–4442 (2005).
16. X. D. Hoa, A. G. Kirk, and M. Tabrizian, "Towards integrated and sensitive surface plasmon resonance biosensors: a review of recent progress," Biosens. Bioelectron. **23**(2), 151–160 (2007).
17. K. H. Yoon, M. L. Shuler, and S. J. Kim, "Design optimization of nano-grating surface plasmon resonance sensors," Opt. Express **14**(11), 4842–4849 (2006).
18. D. C. Cullen, and C. R. Lowe, "A direct surface plasmon-polariton immunosensor: Preliminary investigation of the non-specific adsorption of serum components to the sensor interface," Sens. Actuators B Chem. **1**(1-6), 576–579 (1990).
19. M. Vala, J. Dostalek, and J. Homola, "Diffraction grating-coupled surface plasmon resonance based on spectroscopy of long-range and short-range surface plasmons," Proc. SPIE **6585**, 658522 (2007).
20. C. J. Alleyne, A. G. Kirk, R. C. McPhedran, N. A. P. Nicorovici, and D. Maystre, "Enhanced SPR sensitivity using periodic metallic structures," Opt. Express **15**(13), 8163–8169 (2007).
21. J. M. Brockman, and S. M. Fernandes, "Grating-coupled surface plasmon resonance for rapid, label-free, array based sensing," Am. Lab. **33**, 37–41 (2001).
22. R. Baggio, G. J. Carven, A. Chiulli, M. Palmer, L. J. Stern, and J. E. Arenas, "Induced fit of an epitope peptide to a monoclonal antibody probed with a novel parallel surface plasmon resonance assay," J. Biol. Chem. **280**(6), 4188–4194 (2005).
23. J. Dostalek, J. Homola, and M. Miler, "Rich information format surface plasmon resonance biosensor based on array of diffraction gratings," Sens. Actuators B Chem. **107**(1), 154–161 (2005).
24. D. Y. Kim, "Effect of the azimuthal orientation on the performance of grating-coupled surface-plasmon resonance biosensors," Appl. Opt. **44**(16), 3218–3223 (2005).
25. F. Romanato, K. H. Lee, H. K. Kang, C. C. Wong, Y. Zong, and W. Knoll, "Azimuthal dispersion and energy mode condensation of grating-coupled surface plasmon polaritons," Phys. Rev. B **77**(24), 245435–245441 (2008).
26. C. D. Bain, E. B. Troughton, Yu.-T. Tao, J. Evall, G. M. Whitesides, and R. G. Nuzzo, "Formation of monolayer films by the spontaneous assembly organic thiols from solution onto gold," J. Am. Chem. Soc. **111**(1), 321–335 (1989).
27. B. Thomas, O. Reilly, and I. H. I. Smith, "Linewidth uniformity in Lloyd's mirror interference lithography systems," J. Vac. Sci. Technol. B **26**(6), 2131–2134 (2008).
28. F. Schreiber, "Structure and growth of self-assembling monolayers," Prog. Surf. Sci. **65**(5-8), 151–257 (2000).
29. X. F. Ang, F. Y. Li, W. L. Tan, Z. Chen, C. C. Wong, and J. Wei, "Self-assembled monolayer for reduced temperature direct metal thermocompression bonding," Appl. Phys. Lett. **91**(6), 061913 (2007).

1. Introduction

Surface Plasmon Polaritons (SPP) are electromagnetic waves coupled with surface plasma charge oscillations that propagate along the metal/dielectric interface. Due to its non-radiative nature, SPP can be excited by an incident EM-wave illuminating the metal surface (Surface Plasmon Resonance - SPR) only in proper configurations such as prism-coupling and grating-coupling setup [1]. The resonance condition is extremely sensitive to the changes in refractive index on the metal film within a thickness comparable to the vertical extinction length of SPP [2]. Due to these properties, SPR reveals itself as a useful instrument for the study of surface optical properties and it is a highly suitable candidate as a sensor for liquid or gas solutions [3–5] and surface chemistry [6].

Currently, several groups are using different SPR approaches to detect the change of refractive index [7–10]. Sensors using prism-coupled SPR (PCSPR) with Kretschmann configuration [11] typically show refractive index sensitivity for typical angular interrogation architecture that ranges between 50 and 150°/RIU [12,13], with higher sensitivity at shorter wavelengths [14]. However, PCSPR sensors suffer from cumbersome optical alignment [15] and are not amenable to miniaturization and integration [16].

Another common way for SPR excitation is to use a metallic grating. Grating coupled SPR (GCSPR) sensors with either wavelength or angular interrogation have been demonstrated to have sensitivity 2-3 times lower than PCSPR [17,18]. However, GCSPR has the intrinsic possibility to be used with different sensing architectures and interrogation systems. A parallel SPR angular detection was shown by Unfrict *et al.* to have the possibility for multi detection for proteomic multiarray. Homola's group demonstrated an SPR biosensor with a refractive index sensitivity of 695 nm/RIU by using wavelength interrogation, exploiting the advantages of both long-range and short-range surface plasmons

excited simultaneously on a diffraction grating [19]. Most recently, Alleyne [20] has exploited the generation of an optical band gap in GCSPR by using prism-coupled to achieve sensitivity down to 680°/RIU by bandgap-assisted GCSPR. A miniaturized GCSPR sensor implemented with a CCD allowed detection sensitivity of 50°/RIU over 200 sensing parallel channels [21–23].

To our knowledge, little work has been done to study the effects of rotating the grating substrate itself [24]. Recently, our group has shown that the number of excited SPP modes in GCSPR is related to the azimuthal angle of the grating. The higher the azimuthal angle, the larger is the number of excited SPP modes [25]. The SPP propagation direction can be controlled by rotating the grating azimuthally and double SPP excitation by a single wavelength is possible when the grating azimuthal rotation is larger than a specific angle. Under this condition, a small change in refractive index induces a much larger change in reflectivity, resulting in a higher sensitivity (more than 10 fold increase) than that for the non-rotated case. Here, we show that a self-assembled monolayer of dodecanethiol (C12-SAM) molecules, which is only 1.5 nm in optical thickness [26] can be easily detected with an angular shift as large as 3° and an estimated sensitivity larger than 800°/RIU is possible. The experimental data are accompanied by a model description that explain the principle of sensitivity enhancement.

2. Experimental

The 1D sinusoidal grating used in this study, with a period of 487 nm and amplitude of 25 nm, was generated by interference lithography (IL). The IL system was performed using Lloyd's configuration [27] using a rotating sample holder stage with precision 0.01° in order to have a fine control of the periodicity over the sample. A 40 mW helium cadmium (HeCd) laser from KIMMON emitting a single TEM 00 mode at 325 nm / 441.6 nm is used as the source. The resulting grating has an almost perfect sinusoidal profile with a local roughness of the order of 1 nm rms. Subsequently the grating was formed by thermally evaporating a gold (7nm) /silver (37nm) bi-metallic layer. Silver is preferred because it has a smaller extinction coefficient than gold and therefore suffers less loss during coupling (higher plasmonic coupling efficiency). However a very thin gold coating is used to protect silver from oxidation and provides an inert surface for bio functionalization.

C12-SAM [dodecanethiol ||CH3||CH2|11SH, DDT|□ was deposited on the gold coated grating surface at room temperature in a N2-purged glove box for 24hrs. The spontaneous assembly of the molecules is known to form a densely packed and highly oriented structure on the exposed gold surfaces [28,29]. The details of the SAM deposition is discussed in previous publication [29].

Reflectivity spectra were acquired using a J.A. Woollam Co. VASE instrument with an angular and wavelength spectroscopic resolution of 0.005° and 0.3 nm respectively. The measurements are collected before and after C12-SAM coating on Au grating in air environment. The sample is sitting on the center of rotation of the rotator, thus the location for data collection before and after coating with C12-SAM is not changed with azimuthal rotation.

Incoming light with a $\vec{k}_{ph}$ wave-vector forms an angle θ with the normal z-axis. Measurements are taken in a $\theta/2\theta$ symmetric reflectivity configuration, with θ scanned from 15° to 80° with a step size of 0.5°, using a 75W Xe lamp, monochromatized between 590 nm and 800 nm in steps of 4 nm. In our experimental method, the scattering plane is fixed and the gratings are mounted on a sample holder that can be rotated azimuthally to define the φ angle. Grating orientations used in this experiment were 0° and 60°. The grating lattice period has been determined in 487.3 nm using asymmetric diffraction configuration.

3. Results

The experimental evidence of the azimuthal rotation effect in enhancing the SPR sensitivity is shown in Fig. 1 where reflectivity spectra have been collected at different wavelengths. As a reference, we first report the reflectivity spectra using GCSPR at conventional $\varphi = 0°$ as shown in Fig. 1(a). In this configuration the difference in the reflectivity SPP minima before and after C12 functionalization, $\Delta\theta$, is typically less than 0.05 °. On the contrary, when the grating is azimuthally rotated to an angle of about 60 ° ($\varphi = 61.58°$ in our case), large angular differences, $\Delta\theta$, can be observed between reflectivity dips (Fig. 1(b)). The $\Delta\theta$ differences are of the order of 1.8° but can reach values up to 3 ° as for the case of $\lambda = 618$ nm. The occurrence of double SPP reflectivity dips for a single incident wavelength is due to double matching in the momentum conservation condition, as discussed in our previous publication [25]. By increasing the wavelength from 606 nm to 618 nm, the two resonance dips in the reflectivity spectra come closer together until they merge together into one broad dip at 620 nm. Further increase of wavelength reduces the resonance strength until SPR completely vanishes.
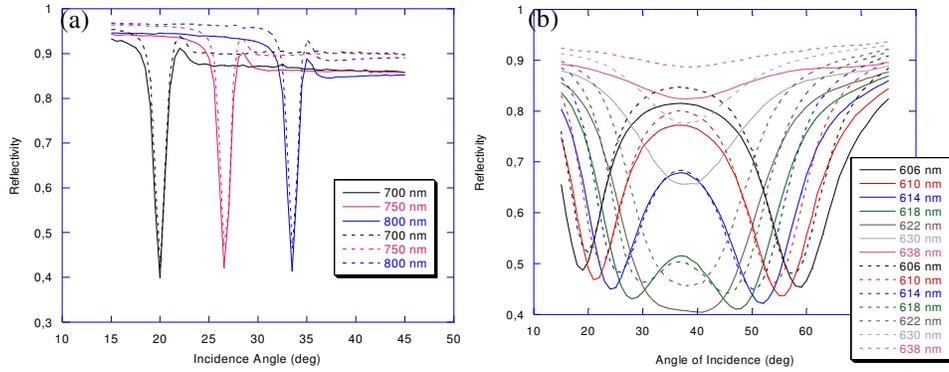

Fig. 1. Comparison of SPR spectrum between uncoated (solid line) and C12-coated (dashed line) Au grating. (a) Grating with $\varphi = 0°$ (conventional mounted grating), where different line colors correspond to different incident wavelengths; and (b) $\varphi = 60°$ (2 SPPs by single wavelength excitation condition), different colors of line represent difference incident wavelength.

4. Analysis and discussion

The analysis of the wave-vector components allows a description of double SPP excitation using the schematic shown in Fig. 2. The excitation of SPPs on a grating is achieved when the on-plane component of the incident light wave-vector and the diffracted SPP wave-vector $\vec{k}_{sp}$ match the momentum conservation condition:

$$\vec{k}_{sp} = \vec{k}_{ph_{\parallel}} \pm m\vec{g} \qquad (1)$$

where $\vec{k}_{ph_{\parallel}} = \dfrac{2\pi}{\lambda}(-\sin\theta_{in}, 0)$, θ_{in} is the angle of incidence, the crystal momentum is $\vec{g} = \dfrac{2\pi}{\Lambda}(\cos\varphi, \sin\varphi)$ whose rotation is measured by φ, and Λ is the grating pitch. Only the first diffraction order (m = 1) is used because in our case, $\vec{g}$ is always greater than $k_{ph_{\parallel}}$.

All quadrants of the circle can be explored for SPP excitation as long as Eq. (1) is satisfied. For symmetry reason, only k_y positive half space is shown.
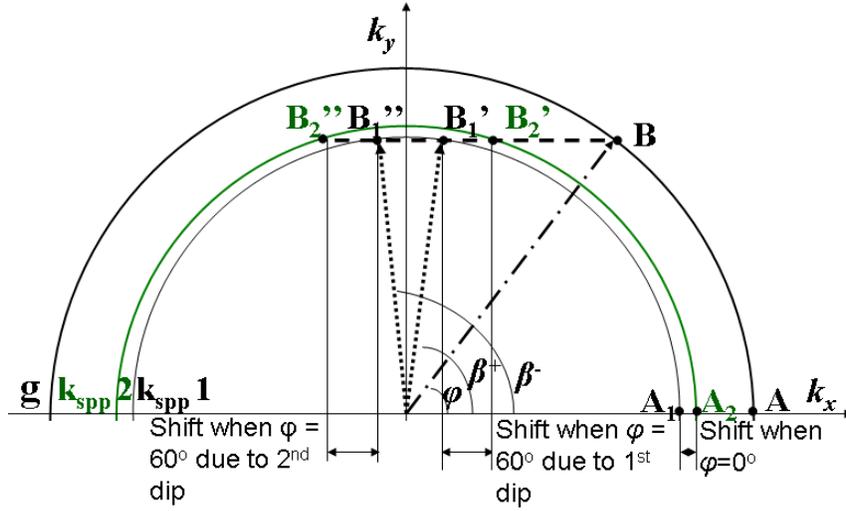

Fig. 2. Schematic represents wave-vectors combination. The large circle represents equi-magnitude $\vec{g}$ vectors. The smaller black and green circles represent equi-magnitude vectors before, ($\vec{k}_{spp1}$), and after ($\vec{k}_{spp2}$), the surface functionalization with C12 SAM. The dashed lines represent a photon wave-vector and the dotted lines represent the SPP propagation direction, β. The letters A and B represent the $\vec{g}$ vector with azimuthal rotation $\varphi = 0°$ and $\varphi = 60°$ respectively. The capital letters with the primes represent the intersection of the photon wave-vector with the SPP semicircles.

The largest circle in k-space represents equi-magnitude $\vec{g}$ vectors at different azimuthal orientation. The two smaller circles represent all possible $\vec{k}_{sp}$ vectors with equal magnitude respectively before and after C12 surface functionalization and whose modulus is given by

$$k_{SPP} = k_{ph}\sqrt{\frac{\varepsilon_M \varepsilon_D}{\varepsilon_M + \varepsilon_D}} = k_{ph}M \qquad (2)$$

where ε_M and ε_D are the dielectric constants of the metal and the dielectric medium respectively. After the coating, the SPP modulus increases because of the small increase in ε_D due to the surface SAM functionalization with C12.

The dashed line at the tip of the circle of radius $\vec{g}$ represents the x component of the photon wave-vector $k_{ph_\parallel}$, the only component that participates in SPP excitation. The line is scaled linearly in $\sin\theta_{in}$ such that the full length of the line at the incident angle θ_{in} of 90° corresponds to the maximum value of $k_{ph_\parallel}$.

The intersections of the $k_{ph_\parallel}$ dashed horizontal line with the smaller k_{spp} circle determine the conditions for which Eq. (1) is satisfied and allows identification of both

incident angle θ_{in} for SPP resonance excitation and SPP propagation direction, β. We consider first the case of the uncoated sample - the smallest of the semicircles. For example, point B on the $\vec{g}$ circle is identified by the azimuthal angle φ and allows the excitation of SPP at two possible conditions: $B_1^{'}$ and $B_1^{''}$, with β^+ and β^-, respectively. Within the double SPP range (point B), a small increment in wavelength makes the points $B_1^{'}$ and $B_1^{''}$ merge, to form a very broad resonance as shown by wavelength dependence of the reflectivity spectra (Fig. 1(b)). On the contrary, at $\varphi = 0°$ (point A) it is clear that the photon wave-vector can intersect the SPP circle only in the first quadrant but not the second, thus exciting only a single SPP for each wavelength (Fig. 1.).

The same understanding is applicable for light exciting SPP on the C12 coated sample. Due to larger k_{spp}, different excitation condition is expected. The intersection points changes from $B_1^{'}$ and $B_1^{''}$ to $B_2^{'}$ and $B_2^{''}$ and from A_1 to A_2. The sensitivity of the GCSPP is higher at high azimuthal angles because the condition for double SPP excitation around the circumference of the k_{spp} circle generates a shifts in k-space between points $B_1^{'}$ and $B_2^{'}$, which is much larger than that between points A_1 and A_2 provided by a single SPP excitation condition for $\varphi = 0°$.

The estimated refractive index sensitivity, S, of this configuration can be defined as:

$$S = \frac{\partial \theta}{\partial n} = \frac{\partial \theta}{\partial k_{ph_x}} \frac{\partial k_{ph_x}}{\partial k_{SPP}} \frac{\partial k_{SPP}}{\partial n} \qquad (3)$$

In order to calculate S, we assume the rippling amplitude, δ, of the grating is so shallow ($\delta/\Lambda = 0.05$ in our case) that the dispersion curve of SPP traveling at the metal-dielectric interface of a grating can be approximated by the case of a flat sample as described by Eq. (2). With Fig. 2 as a reference, the analytical expression for the sensitivity in angular interrogation can be found as:

$$S = -\frac{1}{\cos \theta_r} \left(\frac{M}{n_0} \right)^3 \frac{\sqrt{\frac{1}{\Lambda^2} + \frac{\sin^2 \theta}{\lambda^2} - \frac{2\cos \phi \sin \theta}{\Lambda \lambda}}}{\frac{\cos \phi}{\Lambda} - \frac{\sin \theta}{\lambda}} \qquad (4)$$

where M is defined in Eq. (2), n_0 is the refractive index of the surrounding dielectric medium, λ is the incident wavelength and θ_r is the resonance angle that is equal to

$$\theta_r = \sin^{-1} \left(\frac{\lambda}{\Lambda} \cos \phi \mp \sqrt{M^2 - \left(\frac{\lambda}{\Lambda} \right)^2 \sin^2 \phi} \right) \qquad (5)$$

The functional behavior of sensitivity for the first and second SPP dip is shown in Fig. 3 for a typical wavelength of $\lambda = 606$ nm. Both the sensitivities diverge when ϕ approaches its critical value ϕ_{MAX}, i.e. the maximum ϕ angle that supports SPP resonances. In this configuration, incident photon momentum is tangential to the k_{spp} circle and its length equals to the k_x-component of the grating momentum in so that the denominator of the third term in Eq. (4) becomes null. Another condition for second dip sensitivity singularity is when the φ approaches critical azimuthal angle, φ_c, necessary to excite double SPP resonances, namely when the full length of the incident photon momentum is required to intersect the edge of the k_{spp} circle. Since the incident angle $\theta_{in} = 90°$, $\cos\theta$ in the denominator of the first term Eq. (4) approaches 0 and S diverges.
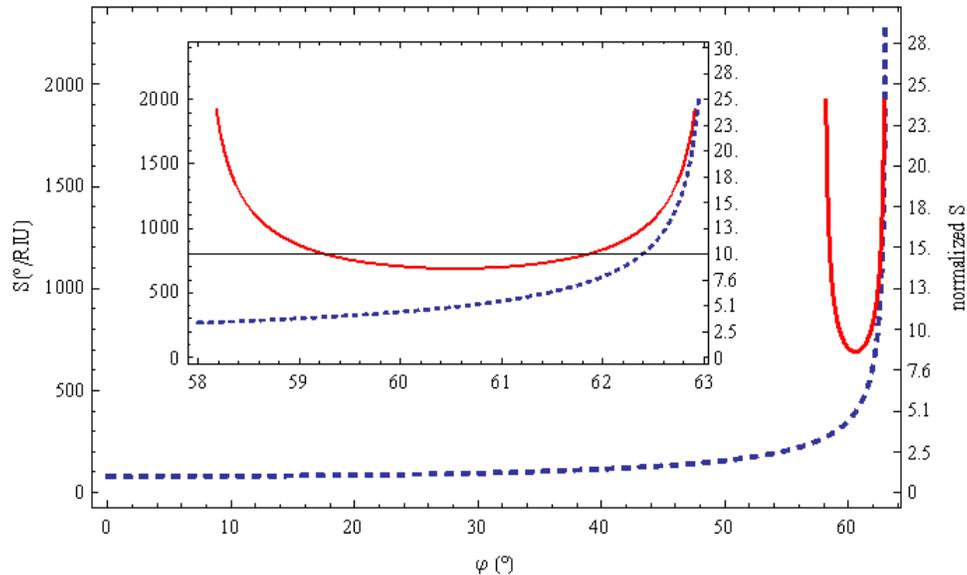
Fig. 3. Sensitivity, *S* as a function of grating azimuthal angle, *φ* for the two dips for the SPR sensor with angular interrogation. The right y-scale refers to sensitivity values normalized to the first dip sensitivity at *φ = 0 (S_r = S/S_1(0))*. In the subset figure, more detail is shown.

Although *φ* close to the critical values provides a great enhancement in S (up to 2400 °/RIU, 35 times higher than φ = 0°), these configurations should be avoided because of experimental limits. For $\varphi \cong \varphi_c$, θ_r becomes large (θ>70°) and broad, becoming impossible to resolve the SPP minimum. In addition, when $\varphi \cong \varphi_{MAX}$, the two resonance dips merge into a single broad dip which makes the two minima indistinguishable. Thus only limited parts of the azimuthal angular range are suitable for enhancing sensitivity significantly. The best conditions correspond to the middle of the "U-shape" of second dip functional behavior (inset of Fig. 3) where the sensitivity ranges from 900 to 1100 °/RIU, about 15 times higher than φ = 0° whose value is 67°/RIU. The sensitivity computed for the first SPP dip is smaller all over this range but it still provides values of the order of 500°/RIU.

The experimental determinations of the wavevector k_{ph} of the incoming light necessary for the SPP excitation have been successfully fitted with the help of Eq. (1), using as fitting parameters only the effective index of refraction and azimuthal angle. After surface functionalization we have determined a total increment in index of refraction equal to $\Delta n = 0.00357 \pm 0.00007$ RIU. This is a value that agrees with the estimation of $\Delta n = 0.0038$ RIU performed for effective refractive index change generated by a full surface coverage of close-packed self assembled C12 molecules, considering their length = 1.488 nm and dielectric constant $\varepsilon_{C12} = 2.205$. Also the theoretical sensitivity determination is in good agreement with the experimental determination obtained as a ratio between $\Delta\theta$, the angular differences before and after C12 coating and the Δn determination as shown in Fig. 4(a). The average experimental sensitivity is of the order of 520 °/RIU for the first dip and reaches maximum values of 857 °/RIU for the second dip.

The final error of the refractive index determination has been estimated on the basis of chi-square minimization based on *a priori* determination of the SPP angular position. The

reflectivity minima of this preliminary data set have been determined with a typical uncertainty of ± 0.07° deg. However the *a posteriori* determination of the SPP angular average deviation with respect to the dispersion curve best fit is much smaller, on the order of 0.015°, as can be confirmed by a simple graphical inspection. Taking into account this more realistic value for the final evaluation of the uncertainty, the value of $\delta\Delta n$ is 7×10^{-5} RIU. However, because our experimental system has an instrumental resolution of 0.001°, we believe it will be possible to greatly decrease the present angular uncertainty by increasing the statistical signal-to-noise ratio and using appropriate algorithms for data analysis. We expect that experimental uncertainties of Δn on the order of $\pm 5 \times 10^{-7}$ RIU is achievable.

In order to better describe the detection improvement given by azimuthal rotation, we have also measured the typical figure of merit for angular and yield interrogation respectively defined as:

$$FOM_{ang} = \frac{S}{\Delta\theta_{FWHM}} = \frac{\left(\partial\theta/\partial n\right)}{\Delta\theta_{FWHM}} \tag{6}$$

$$FOM_Y = \frac{1}{\Delta n}\frac{\left(Y_{coat} - Y_{uncoated}\right)}{Y_{uncoated}} \tag{7}$$

where S is the sensitivity given by Eq. (4), $\Delta\theta_{FWHM}$ is the angular full width at half maximum of the reflectivity minima, whereas Y_{coat} and Y_{uncoat} are the minimum yield of the reflectivity spectra collected before and after C12 functionalization at SPR resonances. Figure 4(b) shows the angular and yield FOM at zero and after the azimuthal rotation for all the reflectivity spectra. It clearly appears an enhancement of both the figures of merit after the azimuthal rotation that amounts up to a factor 4 and 10 for the angular and yield FOM respectively. This means that the distance between two dips, before and after the functionalization, scales with a factor greater than the enlargment of the reflectivity dip width. Moreover, it must be noticed that the reflectivity yield is even more sensitive than the angular position. It clearly appears from the reflectivity spectra of Fig. 1 that whereas the minimum yield between coated and uncoated are almost the same for zero azimuth, it changes dramatically after azimuthal rotation. Finally, we note that both the angular and the yield FOM have similar functional behavior: they increase approaching the condition of two dips merging when $\beta^+ = \beta^- = 90°$. This is due to the dynamical excitation of the plasmons with different directions. While in the case of the null azimuth the plasmon momentum is collinear with exciting light momentum before and after the C12 functionalization, in the case of the azimuthally rotated grating the plasmons that are excited before and after functionalization have different orientations (in Fig. 2 compare the β angles of B points against A points). A complete analysis comprising both angular and reflectivity yield however involves a full dynamical analysis which exceeds the scope of this preliminary work.
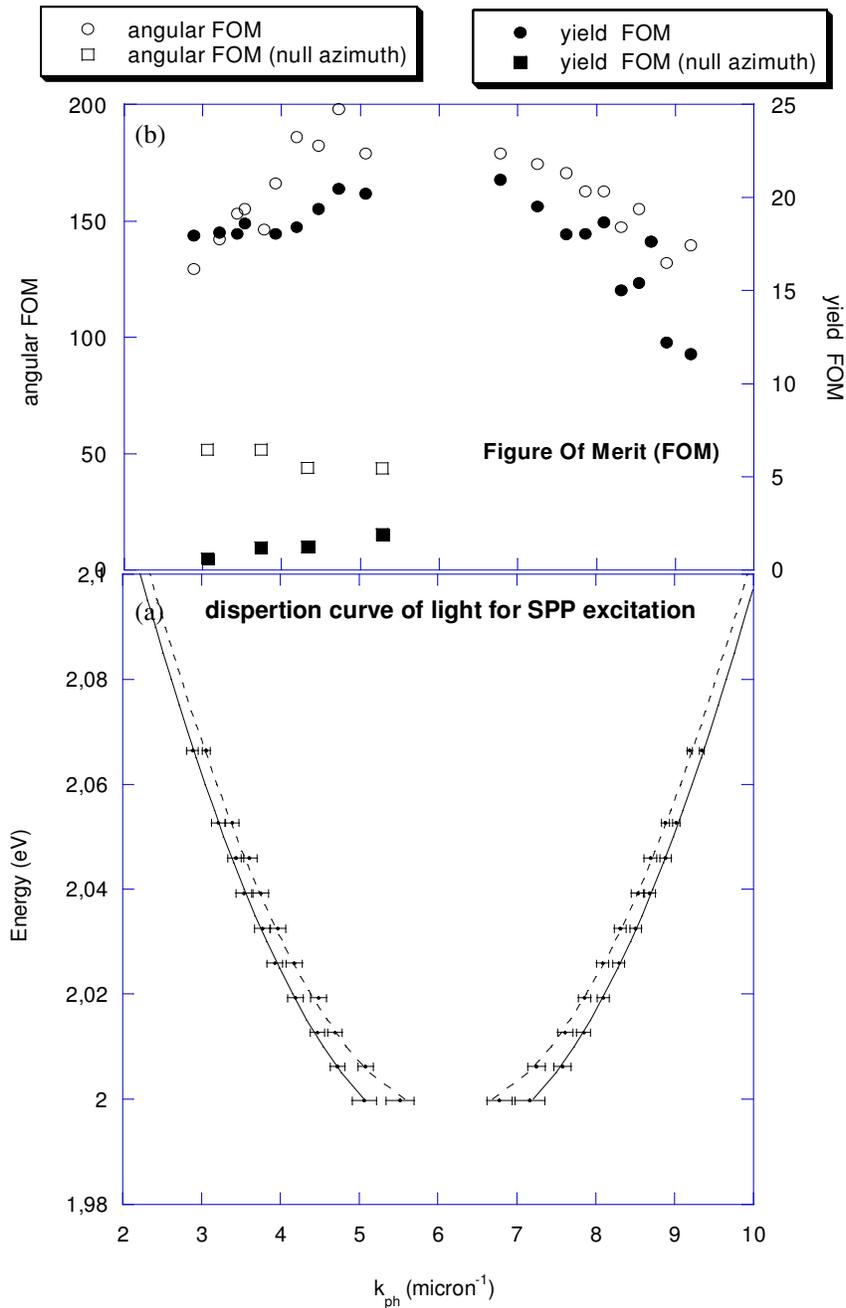
Fig. 4. (b) Figure of merit for angular (•,■) and yield (o, □) interrogation of the SPR reflectivity minima. (a) Energy dispersion curve for the k_{ph} necessary for SPP excitation before (solid line) and after (dashed line) C12 SAM functionalization. The experimental data obtained by the reflectivity minima of Fig. 1 have been fitted using Eq. (1).

5. Conclusion

In summary, we have shown that an enhancement in sensitivity can be obtained in GCSPR when double SPPs are excited after azimuthal rotation of the grating. The difference between uncoated and C12 SAMs coated metallic gratings is easily detectable in the vicinity of the double SPP condition. The shift in resonance angle detected is as large as 3° which is one order of magnitude higher than conventional prism-based SPR. In addition, the calculated sensitivity of this method is greater than 800 $^{\circ}$/RIU, one order of magnitude higher than conventional mounted grating ($\varphi = 0°$).